Published in final edited form as:
Arterioscler Thromb Vasc Biol. 2001 September ; 21(9): 1556–1560.

In Vivo Magnetic Resonance Imaging of Experimental Thrombosis in a Rabbit Model

Michael T. Johnstone, **René M. Botnar**, **Alexandra S. Perez**, **Robert Stewart**, **William C. Quist**, **James A. Hamilton**, and **Warren J. Manning**
From the Department of Medicine, Cardiovascular Division (M.T.J., R.M.B., A.S.P., W.J.M.), and the Departments of Radiology (W.J.M.), Surgery (R.S.), and Pathology (W.Q.), Beth Israel Deaconess Medical Center and Harvard Medical School, and the Department of Biophysics (J.H.), Boston University School of Medicine, Boston, Mass.

Abstract

The process of atherosclerotic plaque disruption has been difficult to monitor because of the lack of an animal model and the limited ability to directly visualize the plaque and overlying thrombus in vivo. Our aim was to validate in vivo magnetic resonance imaging (MRI) of the thrombus formation after pharmacological triggering of plaque disruption in the modified Constantinides animal model of plaque disruption. Atherosclerosis was induced in 9 New Zealand White male rabbits (3 kg) with aortic balloon endothelial injury followed by a high cholesterol (1%) diet for 8 weeks. After baseline (pretrigger) MRI, the rabbits underwent pharmacological triggering with Russell's viper venom and histamine, followed by another MRI 48 hours later. Contiguous cross-sectional T2-weighted fast spin echo images of the abdominal aorta were compared by histopathology. In all animals, aortic wall thickening was present on the pretrigger MRI. On MRIs performed 48 hours after triggering, a histologically confirmed intraluminal thrombus was visualized in 6 (67%) of the 9 animals. MRI data correlated with the histopathology regarding aortic wall thickness ($R = 0.77$, $P < 0.0005$), thrombus size ($R = 0.82$, $P < 0.0001$), thrombus length ($R = 0.86$, $P < 0.005$), and anatomic location ($R = 0.98$, $P < 0.0001$). In vivo, MRI reliably determines the presence, location, and size of the thrombus in this animal model of atherosclerosis and plaque disruption. The combination of in vivo MRI and the modified Constantinides animal model could be an important research tool for our understanding of the pathogenesis of acute coronary syndromes.

Keywords

atherosclerosis; plaque; MRI; thrombosis

Acute cardiovascular events remain the leading cause of death in industrialized nations.[1,2] The underlying mechanism of most acute coronary syndromes is the disruption of an atherosclerotic coronary plaque with an overlying thrombus.[3–6] Although the accepted gold standard for the detection of this disease process is coronary angiography, this technique is invasive, gives little information regarding the composition of the atheromatous wall, and

Correspondence to Michael T. Johnstone, MD, Beth Israel Deaconess Medical Center Cardiovascular Division, Kennedy Building, 5th Floor, Boston, MA. 02215. mjohnst1@caregroup.harvard.edu.

Reprint requests to René Botnar, PhD, Beth Israel Deaconess Medical Center Cardiovascular Division, 330 Brookline Ave, Boston, MA. 02215. rbotnar@caregroup.harvard.edu

frequently cannot detect the presence of a thrombus or differentiate a thrombus from underlying atheroma.[7,8] MRI is a noninvasive modality that has been shown to detect atheromatous plaques in the large arteries of experimental[9–14] and human[15–19] atherosclerosis but has not been applied to acute coronary syndromes. Using a modified Constantinides model of plaque disruption,[20,21] we sought to determine whether MRI could detect a thrombus overlying an atherosclerotic plaque, a frequent occurrence in plaque disruption.

Methods

Rabbit Housing and Diet

Nine adult male New Zealand White rabbits weighing ≈3 kg (Millbrook Immunoserv, Amherst, Mass) were continuously housed at the hospital's animal care facilities. All studies were performed under the approval of the hospital Animal Care and Use Committee on Animal Investigations.

The study protocol is summarized in Figure 1. Animals were fed a 1% high cholesterol diet incorporated into the rabbit chow (Purina modified 1% cholesterol diet 5736C-G) beginning immediately after balloon injury and continuing for 8 weeks. Fasting serum cholesterol values were obtained before balloon injury and before "triggering."

Balloon Injury and Endothelial Denudation

Rabbits were anesthetized with ketamine (35 mg/kg IM), xylazine (5 mg/kg IM), and acepromazine (0.75 mg/kg IM). Anesthesia was maintained during the procedure with isoflurane inhalation via mask. Balloon-induced arterial wall injury of the aorta was performed with a 3F Fogarty catheter introduced through a right femoral artery cutdown. The catheter was first advanced 30 cm, to a level just above the aortic valve. The balloon was then inflated with 0.3 mL saline, and the catheter was gently retracted to the iliofemoral artery. This procedure was performed 3 times in each rabbit. The catheter was then removed, and the incision was sutured closed.

Pharmacological Triggering and Euthanasia

After endothelial denudation and 8 weeks of high cholesterol diet, plaque disruption was triggered by using Russell's viper venom (0.15 mg/kg IP, Sigma Chemical Co), followed 30 minutes later by histamine (0.02 mg/kg IV) at 48 and at 24 hours before euthanasia.

Immediately before euthanasia, heparin sulfate (10 U/kg IV) was given to prevent postmortem clotting. Euthanasia was performed by using ketamine (35 mg/kg IM) and xylazine (5 mg/kg IM), followed by a bolus injection of sodium pentobarbital (100 mg/kg IV).

MRI Study Protocol

Rabbits were sedated by using ketamine (35 mg/kg IM), xylazine (5 mg/kg IM), and acepromazine (0.75 mg/kg IM). Rabbits were positioned prone on the MRI table with the ECG leads on the anterior hemithorax for R-wave detection. All scans were performed on a 1.5-T Philips Gyroscan ACS-NT MR scanner (Philips Medical Systems) by use of a 5-element cardiac phased-array coil for signal reception and an advanced cardiac software patch (CPR6). After balloon injury of the thoracic and abdominal aorta and a subsequent 8-week high cholesterol diet, animals underwent the "pretrigger" MRI examination (Figure 1). The abdominal aortic localizer consisted of a fast multislice multistack (transverse, sagittal, and coronal) segmented Turbo Field Echo (TFE) localizer scan of the abdomen. (repetition time 8 ms, echo time 2 ms, flip angle 30°, slice thickness 3 mm, field of view 180 × 180

mm, and matrix 256 × 64). From transverse images of the abdominal aorta, a second coronal scout with a reduced slice thickness (1 mm) was obtained along the major axis of the abdominal aorta. The right renal artery visible on a scout image was then used as a landmark to position the most cranial slice for T2-weighted cross-sectional imaging of the abdominal aorta from the right renal artery to the distal aortic bifurcation. For transverse aortic imaging, fat-suppressed T2-weighted fast spin echo scan (24 contiguous slices, repetition time 6 RR intervals, echo time 60 ms, slice thickness 5 mm, field of view 120 × 96 mm, and matrix 512 × 205) that allowed the assessment of cross-sectional views of the aortic vessel wall was performed. In-plane spatial resolution was 230 × 470 μm. The echo train length and spacing were 12 and 9.2 ms, respectively; this echo spacing was the minimum for the chosen resolution and slice thickness. The total imaging time for the T2-weighted scan was ≈11 minutes, 20 seconds (heart rate 150 bpm).

The same MRI protocol was repeated 48 hours after the first triggering dose (“posttrigger”). After the posttrigger MRI examination, the animals were euthanized in the manner described above.

Tissue Preparation

After euthanasia of the animals, 6 rabbits were perfusion-fixed by using 10% formalin acetate for a minimum of 2 hours. The aorta, from the aortic valve to the femoral bifurcation, was removed, and 2.5-mm serial sections of the aorta were cut and catalogued. These samples then underwent additional fixation overnight in formalin, followed by overnight tissue processing and dehydration. The samples were embedded in paraffin the following day. The serial cross sections were processed for general histological staining with hematoxylin-phloxine-saffron (HPS).

The aortas from the remaining rabbits were immediately excised and cut into 16 serial 2.5-mm sections, with alternative sections embedded in paraffin and catalogued. These specimens were embedded in OCT compound (Tissue Tek, Fisher Scientific), snap-frozen, and stored at −80°C for later general histological staining, as described above.

Histological Analysis

Identification of Disrupted Plaques—Sections stained with HPS were analyzed for the presence of disrupted plaques. Disrupted plaques were defined as those plaques with an overlying premortem thrombus. Plaques that had no overlying thrombus were defined as nondisrupted plaques.

Determination of Atherosclerotic Burden and Presence of Thrombus—Percentage aortic wall thickness [(outer wall area–area of lumen)/(outer wall area) × 100%] and the percent stenosis of the lumen area [area of thrombus/(area of lumen) × 100%] were determined on pretrigger magnetic resonance images by manually tracing the inner and outer vessel wall. These calculations were performed on the pretrigger images because it was hard to distinguish between the thrombus and the luminal surface of the aortic wall. The corresponding histological sections of the aorta stained with HPS were put on a projecting microscope (Microprojector/model 1202, Carl Zeiss, Inc) and were projected onto a digitizing tablet. The luminal, intimal, medial, and outer wall areas were manually traced and quantified by using NIH Image Analysis Software program (Scion Image, Release 3b). The percent aortic wall thickness and percent stenosis were determined histologically by the manner described above for MRI. By using the distance from the right renal artery as the point of reference, comparative analyses were performed with the MRI scans at the same level. Because of aortic length shrinkage after removal before perfusion fixation or snap-freezing, the aorta was first stretched to the same length (right renal artery to distal aortic

bifurcation) as the magnetic resonance image obtained by use of pins on a cork board. The length of the aorta was then determined after the pins were removed, and a linear correction factor was calculated. The length of the thrombus was determined by evaluating each of the 2.5-mm sections for the presence of thrombus.

Statistical Analysis

All data are reported as mean ± 1 SD. Comparisons and correlations were made by paired *t* test, least-squares linear regression, and the Fisher exact test, where appropriate. A value of $P \leq 0.05$ was considered significant.

Results

All animals underwent initial balloon injury without complications and recovered uneventfully. The weight of the rabbits at baseline was 3.2 ± 0.4 kg and increased to 3.6 ± 0.3 kg ($P = 0.012$) after the 8-week 1% cholesterol diet period.

Cholesterol Levels

The total serum cholesterol at baseline was 59 ± 11 mg/dL with an LDL cholesterol level of 32 ± 8 mg/dL. After 8 weeks on the 1% cholesterol diet (just before triggering), the serum total cholesterol level had increased to 1885 ± 349 mg/dL ($P < 0.001$), and LDL cholesterol had increased to1421 ± 309 mg/dL ($P < 0.001$).

Rate of Plaque Rupture and Thrombus Formation

Just before euthanasia of the animals, 6 (67%) of the animals had visible evidence of a new aortic opacity on MRI (Figure 2; online Figure I, which can be accessed at http://atvb.aha-journals.org), which was not present in the MRI before triggering, with 2 rabbits having 2 thrombi each, for a total of 8 thrombi. All thrombi had developed in the infrarenal abdominal aorta. On histology, all 9 rabbits had evidence of atherosclerosis, as indicated by intimal thickening.

Comparative Analysis of the Histomorphometric and MRI Features of Aortic Pretriggering and Posttriggering

Representative MRI and histopathology are shown in Figure 2 and online Figure I. Figure 2A and online Figure IA are coronal magnetic resonance reconstructions. Figure 2A shows 2 thrombi; online Figure IA shows 1 thrombus. Cross-sectional magnetic resonance images of the aorta before triggering are shown in Figure 2B and 2C; a thickened aorta with a circular lumen is seen. Similarly, in online Figure IB and IC, MR reconstructions of aortic cross sections from another rabbit before triggering are shown. In determining the thickness of the aortic wall from the histological samples, care was used to exclude the thrombus. The values of percent wall thickness by MRI are closely correlated ($R = 0.77$, $P < 0.001$) with the histological values. The abdominal aorta luminal stenosis was 35.7 ± 5.5% (mean ± SD), whereas the thoracic aorta luminal stenosis was 22.3 ± 2.3% ($P < 0.001$).

Figure 2D and 2E shows posttrigger magnetic resonance images of the aortic cross sections, with each showing a new crescent-shaped mass/thrombus not seen in the pretriggering MRI at the same level (Figure 2B and 2C). The corresponding histological sections, Figure 2F and 2G, respectively, confirm the thrombus within the lumen of the aorta at these levels. A new posttrigger thrombus is also seen in online Figure ID and IE and is confirmed by histological analyses of the corresponding sections (online Figure IF and IG). MRI was able to determine the presence or absence of a thrombus in all animals.

The percent luminal stenosis as a result of the thrombus was determined by comparing posttrigger MRIs with their respective pretrigger MRI. The percent luminal stenosis and MRI had a strong correlation ($R = 0.82$, $P<0.001$). The thrombus location, defined as the most distal point of the thrombus from the right renal artery, showed excellent correlation ($R = 0.98$, $P<0.001$) between histology and MRI (Figure 3). Similarly, there was a very good correlation ($R = 0.86$, $P = 0.001$) between thrombus length by MRI and histology (Figure 4).

The correlation of the MRI to the histological samples would have been even greater regarding the percent luminal stenosis after triggering ($R = 0.93$) and percent aortic wall thickness ($R = 0.81$) if the frozen samples had not been included in the regression analysis. Eliminating the frozen samples did not affect thrombus location ($R = 0.98$) but did adversely affect the comparative analysis of the thrombus length ($R = 0.72$).

Retrospective assessment of plaque ruptured areas on the pretrigger MRI failed to identify any unique attributes relative to areas of the aorta that did not rupture in terms of wall thickness or morphology.

Discussion

In the present study, which used an atherosclerotic rabbit model of plaque rupture, in vivo MRI was shown to accurately identify new thrombi in rabbits that had undergone pharmacological triggering. There was also excellent correlation between MRI and histology regarding thrombus length and location as well as aortic wall thickness and aortic luminal stenosis. The changes seen between pretrigger and posttrigger MRI confirm that in this model, the development of a thrombus occurs after triggering with Russell's viper venom and histamine.

Recently, there has been considerable interest in the use of MRI for the noninvasive assessment of atherosclerosis because it can evaluate the plaque directly and can potentially determine whether a plaque is vulnerable to disruption. Toussaint et al[16–18] and others[9–15,19] have performed in vivo MRI studies to characterize atherosclerosis in human plaques and animal models. Fayad et al14 and Skinner et al[19] detected thrombi by using MRI in an animal model but did not show prethrombus images for comparison. Having such prethrombus (or pretriggering) images makes the distinction between thrombi and plaques easier and more reliable. Our results confirm the findings of McConnell et al,[9] Fayad et al, 14 and others as to the sensitivity of MRI in the evaluation of aortic wall thickness. Recently, Moody et al,22 who used T1-weighted imaging, detected acute thrombi in the human carotid arteries in those patients having an acute stroke with possible intraplaque hemorrhage, consistent with plaque disruption.

Modified Constantinides Animal Model

The Constantinides animal model is one of the few animal models of acute plaque disruption and thrombosis[19–21,23] and is relatively easy to use. In another animal model of plaque disruption, Skinner et al19 used a double balloon injury of the aorta to induce atherosclerosis in rabbits and found a thrombus overlying a plaque in 1 rabbit. In the original Constantinides model,20 atherosclerosis was induced by a 1% cholesterol diet for two 2-month periods, alternating with 2 months of normal feeding to minimize hepatic failure.21 Over 10% of the rabbits in the original Constantinides model died of hepatotoxicity. The rate of plaque disruption after Russell's viper venom and histamine, defined in the original model as the presence of a platelet-rich thrombus overlying an atherosclerotic plaque, was ≈30%. Abela et al[21] demonstrated that by having the rabbits undergo aortic balloon injury followed by 8 weeks of a 1% cholesterol diet, the rate of plaque disruption after pharmacological triggering was increased to 71%, a value similar to the results (67%) found in the present

study. The balloon injury or modified Constantinides model[21] used in the present study results in more rapid and extensive atherosclerosis, with a higher event rate of plaque disruption than the original Constantinides model. Furthermore, the combination of balloon injury and cholesterol feeding, as was used in the modified Constantinides model, results in lesions that are more uniform in size and distribution and produces plaques that resemble those found in human coronary arteries. 24 The thrombi were platelet rich, which is similar to human arterial thrombi. A major advantage of the use of a rabbit over other animals is that the rabbit's aorta is approximately the same anatomic size as the human coronary artery.

In this model, the degree of atherosclerosis tends to be greater in the abdominal aorta than the thoracic aorta,[25] which might explain why the thrombi in the aorta of the rabbits were consistently located infrarenally but above the aortic bifurcation. The reason for this increased atherosclerosis in the abdominal aorta relative to the thoracic aorta may be due to hemodynamic effects, such as wall shear stress and turbulence. Another possibility is that the abdominal aorta gradually tapers down to the aortic bifurcation. Therefore, the more distal aorta may have sustained more injury relative to the proximal aorta as a result of the fixed size of the inflated balloon relative to the aorta.

Although assumed, until now it had not been demonstrated whether thrombus development occurred before or after the Russell's viper venom and histamine trigger in the modified Constantinides animal model. Our MRI results did not demonstrate thrombi on pretrigger images, confirming the development of a thrombus after requirement of Russell's viper venom and histamine. Plaques vulnerable to disrupt in humans are thought to be minimally stenotic plaques.[4] As indicated by our pretrigger MRI, the degree of stenosis at the site of plaque disruption in these animals is minimal.

Limitations of the Study

There are limitations to the comparative analysis of MRI with the histological sections. The fresh frozen technique is superior to perfusion fixation regarding subsequent immunohistochemical staining.[26] However, compared with the fresh frozen technique, perfusion fixation more favorably preserves the shape of the vessel. This results in cross-sectional tissue shrinkage and shape deformation, which may lead to underestimation of the true lumen size. Furthermore, the ex vivo rabbit aorta is also subject to shrinkage lengthwise after dissection. The accuracy of thrombus location by histology is further compromised by the estimation of the distance of the thrombus from the ends of the 2.5-mm slices. We sought to minimize the impact of shrinkage by performing aortic stretching immediately after euthanasia, making the aorta equal to the length determined by the MRI. We then obtained a length without stretching and applied a linear correction factor.

Several groups have suggested that the relative lipid content is an important factor in determining plaque vulnerability. [3,4] Differentiation of lipid from fibrous or small thrombotic components of the pretrigger plaque with the use of MRI is difficult because of the large pixel size compared with plaque thickness in this model. New intravascular MRI coils may allow for better plaque characterization.27 Unfortunately, such modifications are invasive and, therefore, less attractive. Other possible improvements of MRI techniques (including diffusion weighting,14 high gradient strength,28 and a combination of T2-weighted imaging with 1H spectroscopy29) that may overcome these hurdles remain to be explored. Such advances may allow physicians to better diagnose the long-term risk of chest pain syndromes as well as aid in the ability to determine plaque vulnerability, leading to improved therapeutic options.

Conclusions

In this rabbit model of atherosclerosis and plaque rupture, we demonstrate the ability of in vivo MRI to determine the presence, location, and size of a thrombus in the rabbit aorta after pharmacological triggering. The combination of in vivo MRI and the modified Constantinides animal model may be an important research tool in furthering our understanding and treatment of acute coronary syndromes.

Supplementary Material

Refer to Web version on PubMed Central for supplementary material.

Acknowledgments

This work was supported in part by the National Heart, Lung and Blood Institute grant RO1 HL-61825 and Astra-Zeneca funding to M.T.J. We are grateful to Dr Gary Horowitz, MD, for his excellent technical assistance.

References

1. Lopez AD, Murray CC. The global burden of disease, 1990–2020. Nat Med 1998;4:1241–1243. [PubMed: 9809543]
2. Braunwald E. Shattuck Lecture: cardiovascular medicine at the turn of the millennium: triumphs, concerns, and opportunities. N Engl J Med 1997;337:1360–1369. [PubMed: 9358131]
3. Davies MJ, Thomas AC. Plaque fissuring: the cause of acute myocardial infarction, sudden ischemic death, and crescendo angina. Br Heart J 1985;53:363–373. [PubMed: 3885978]
4. Libby P. Molecular bases of the acute coronary syndromes. Circulation 1995;91:2844–2850. [PubMed: 7758192]
5. Fuster V, Badimon L, Badimon J, Chesebro J. Mechanisms of disease: the pathogenesis of coronary artery disease and the acute coronary syndromes (1). N Engl J Med 1992;326:242–250. [PubMed: 1727977]
6. Fuster V, Badimon L, Badimon JJ, Chesebro JH. The pathogenesis of coronary artery disease and the acute coronary syndromes (2). N Engl J Med 1992;326:310–318. [PubMed: 1728735]
7. Lee RT, Libby P. The unstable atheroma. Arterioscler Thromb Vasc Biol 1997;17:1859–1867. [PubMed: 9351346]
8. Libby P. Lesion versus lumen. Nat Med 1995;1:17–18. [PubMed: 7584941]
9. McConnell MV, Aikawa M, Maier SE, Ganz P, Libby P, Lee RT. MRI of rabbit atherosclerosis in response to dietary cholesterol lowering. Arterioscler Thromb Vasc Biol 1999;19:1956–1959. [PubMed: 10446077]
10. Worthley SG, Helft G, Fuster V, Zaman AG, Fayad ZA, Fallon JT, Badimon JJ. Serial in vivo MRI documents arterial remodeling experimental atherosclerosis. Circulation 2000;101:586–589. [PubMed: 10673247]
11. Worthley SG, Helft G, Fuster V, Fuster V, Fayad ZA, Rodriguez OJ, Zaman AG, Fallon JT, Badimon JJ. Noninvasive in vivo magnetic resonance imaging of experimental coronary artery lesions in a porcine model. Circulation 2000;101:2956–2961. [PubMed: 10869269]
12. Fayad ZA, Nahar T, Fallon JT, Goldman M, Aguinaldo JG, Badimon JJ, Shinnar M, Chesebro JH, Fuster V. In vivo magnetic resonance evaluation of atherosclerotic plaques in the human thoracic aorta: a comparison with transesophageal echocardiography. Circulation 2000;101:2503–2509. [PubMed: 10831525]
13. Fayad ZA, Fuster V, Fallon JT, Jayasundera T, Worthley SG, Helft G, Aguinaldo JG, Badimon JJ, Sharma SK. Noninvasive in vivo human coronary artery lumen and wall imaging using black-blood magnetic resonance imaging. Circulation 2000;102:506–510. [PubMed: 10920061]
14. Fayad ZA, Fallon JT, Shinnar M, Wehrli S, Dansky HM, Poon M, Badimon JJ, Charlton SA, Fisher EA, Breslow JL, et al. Noninvasive In vivo high-resolution magnetic resonance imaging of

atherosclerotic lesions in genetically engineered mice. Circulation 1998;98:1541–1547. [PubMed: 9769308]

15. Pearlman JD, Southern JF, Ackerman JL. Nuclear magnetic resonance microscopy of atheroma in human coronary arteries. Angiology 1991;42:726–733. [PubMed: 1928813]
16. Toussaint JF, LaMuraglia GM, Southern JF, Fuster V, Kantor HL. Magnetic resonance images lipid, fibrous, calcified, hemorrhagic, and thrombotic components of human atherosclerosis in vivo. Circulation 1996;94:932–938. [PubMed: 8790028]
17. Toussaint JF, Southern JF, Fuster V, Kantor HL. T2-weighted contrast for NMR characterization of human atherosclerosis. Arterioscler Thromb Vasc Biol 1995;15:1533–1542. [PubMed: 7583524]
18. Toussaint JF, Southern JF, Kantor HL, Jang IK, Fuster V. Behavior of atherosclerotic plaque components after in vitro angioplasty and atherectomy studied by high field MR imaging. Magn Reson Imaging 1998;16:175–183. [PubMed: 9508274]
19. Skinner MP, Yuan C, Mitsumori L, Hayes CE, Raines EW, Nelson JA, Ross R. Serial magnetic resonance imaging of experimental atherosclerosis detects lesion fine structure, progression and complications in vivo. Nat Med 1995;1:69–73. [PubMed: 7584956]
20. Constantinides P, Chakravarti RN. Rabbit arterial thrombosis production by procedures. Arch Pathol 1961;72:197–208. [PubMed: 13695142]
21. Abela GS, Picon PD, Friedl SE, Gebara OC, Miyamoto A, Tofler GH, Muller JE. Triggering of plaque disruption and arterial thrombosis in an atherosclerotic rabbit model. Circulation 1995;91:776–784. [PubMed: 7828306]
22. Moody AR, Allder S, Lennox G, Gladman J, Fentem P. Direct magnetic resonance imaging of carotid artery thrombus in acute stroke. Lancet 1999;353:122–123. [PubMed: 10023906]
23. Rekhter MD, Hicks GW, Brammer DW, Work CW, Kim JS, Gordon D, Keiser JA, Ryan MJ. Animal model that mimics atherosclerotic plaque rupture. Circ Res 1998;83:705–713. [PubMed: 9758640]
24. Aikawa M, Rabkin E, Voglic SJ, Shing H, Nagai R, Schoen FJ, Libby P. Lipid lowering promotes accumulation of mature smooth muscle cells expressing smooth muscle myosin heavy chain isoforms in rabbit atheroma. Circ Res 1998;83:1015–1026. [PubMed: 9815149]
25. Aikawa M, Voglic SJ, Sugiyama S, Rabkin E, Taubman MB, Fallon JT, Libby P. Dietary lipid lowering reduces tissue factor expression in rabbit atheroma. Circulation 1999;100:1215–1222. [PubMed: 10484543]
26. Haudenschild C, Gould KE, Quist WC, LoGerfo FW. Protection of endothelium in vessel segments excised for grafting. Circulation 1981;64 suppl II:II-101–II-107. [PubMed: 7249310]
27. Correia LC, Atalar E, Kelemen MD, Ocali O, Hutchins GM, Fleg JL, Gerstenblith G, Zerhouni EA, Lima JA. Intravascular magnetic resonance imaging of aortic atherosclerotic plaque composition. Arterioscler Thromb Vasc Biol 1997;17:3626–3632. [PubMed: 9437214]
28. Yuan C, Beach KW, Smith LHJ, Hatsukami TS. Measurement of atherosclerotic carotid plaque size in vivo using high resolution magnetic resonance imaging. Circulation 1998;98:2666–2671. [PubMed: 9851951]
29. Pohost GM, Fuisz AR. From the microscope to the clinic: MR assessment of atherosclerotic plaque. Circulation 1998;98:1477–1478. [PubMed: 9769298]

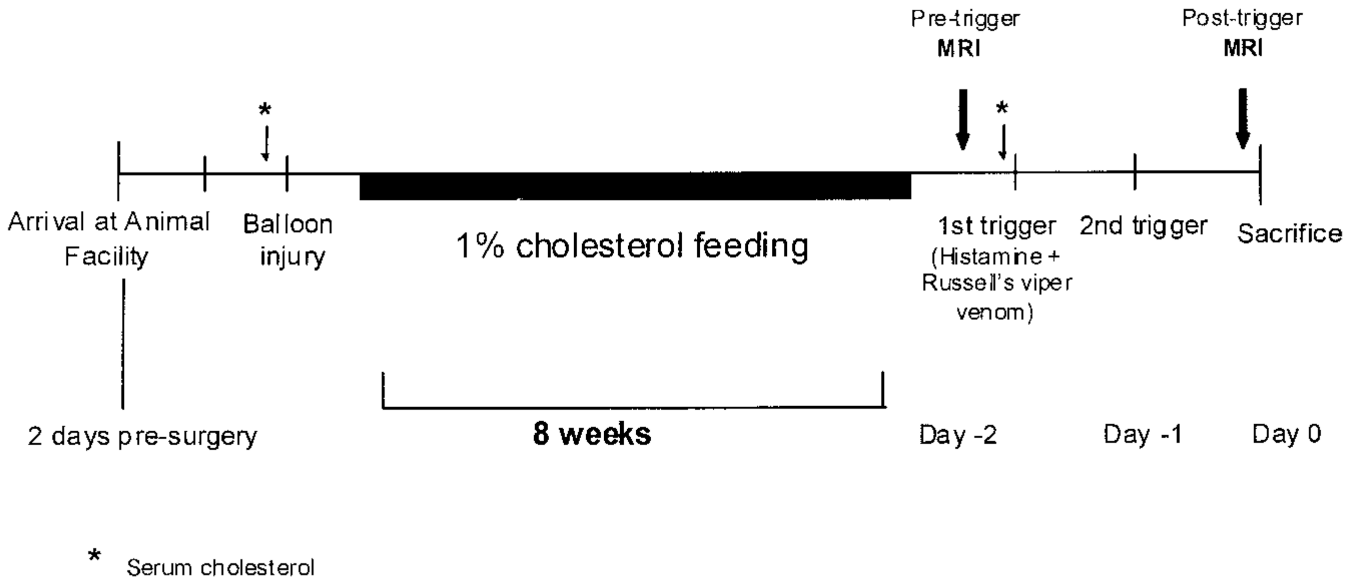

Figure 1.

Schematic diagram of study time line. Balloon injury is followed by 8 weeks of 1% cholesterol feeding. MRI of the rabbit aorta is performed before (pretrigger) the first and after the second (posttrigger) pharmacological triggering MRI. Serum cholesterol is also monitored at baseline and before triggering.

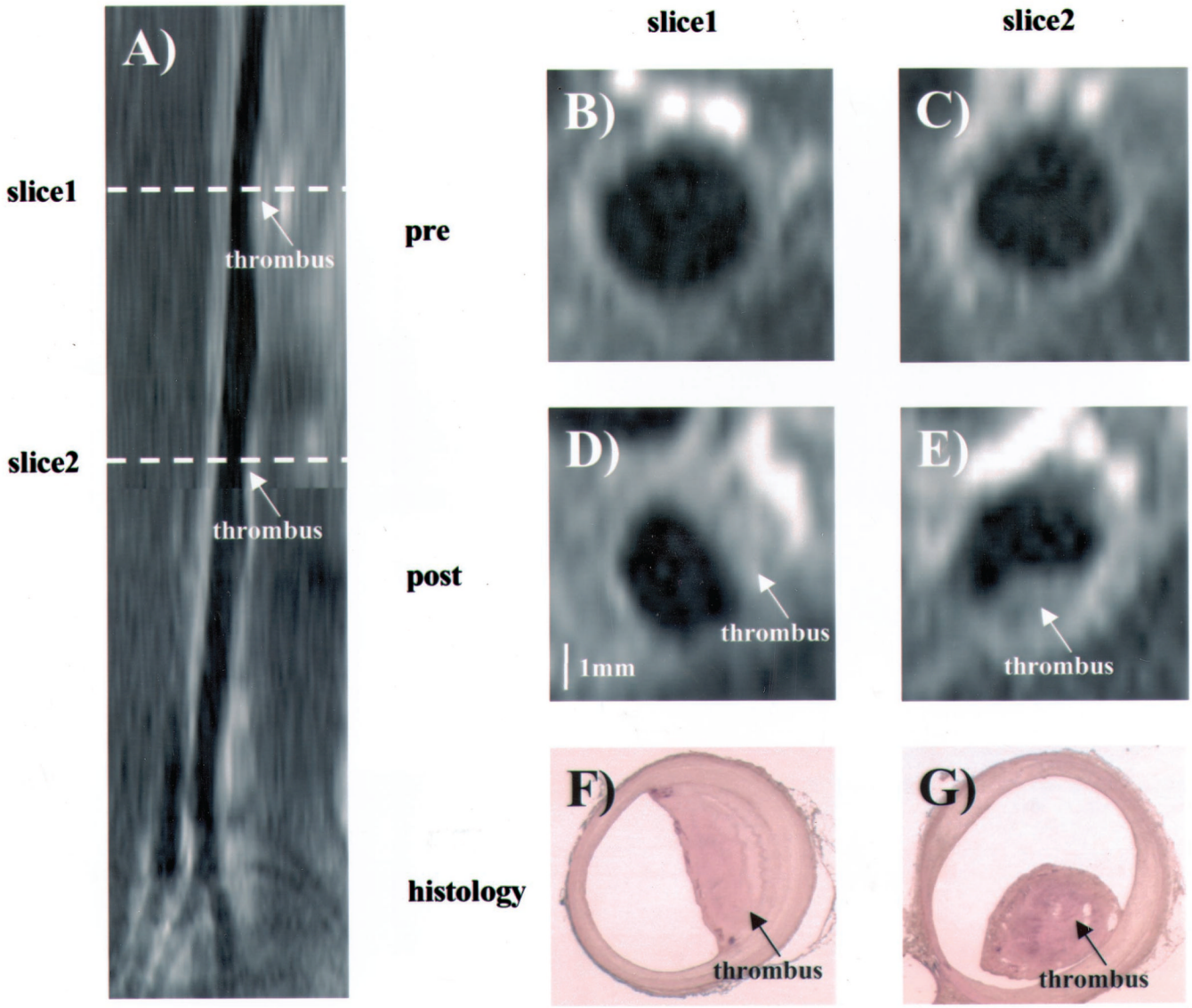

Figure 2.

Coronal magnetic resonance reconstruction (A) and cross-sectional MRI (B through E) of the abdominal aorta of a rabbit that develops a new thrombus. MR images pre- (B and C) and post- (D and E) pharmacologic triggering. Images D and E show new thrombi. Corresponding histopathology of sections is shown (F and G, respectively). An intra-aortic thrombus is shown (arrows).

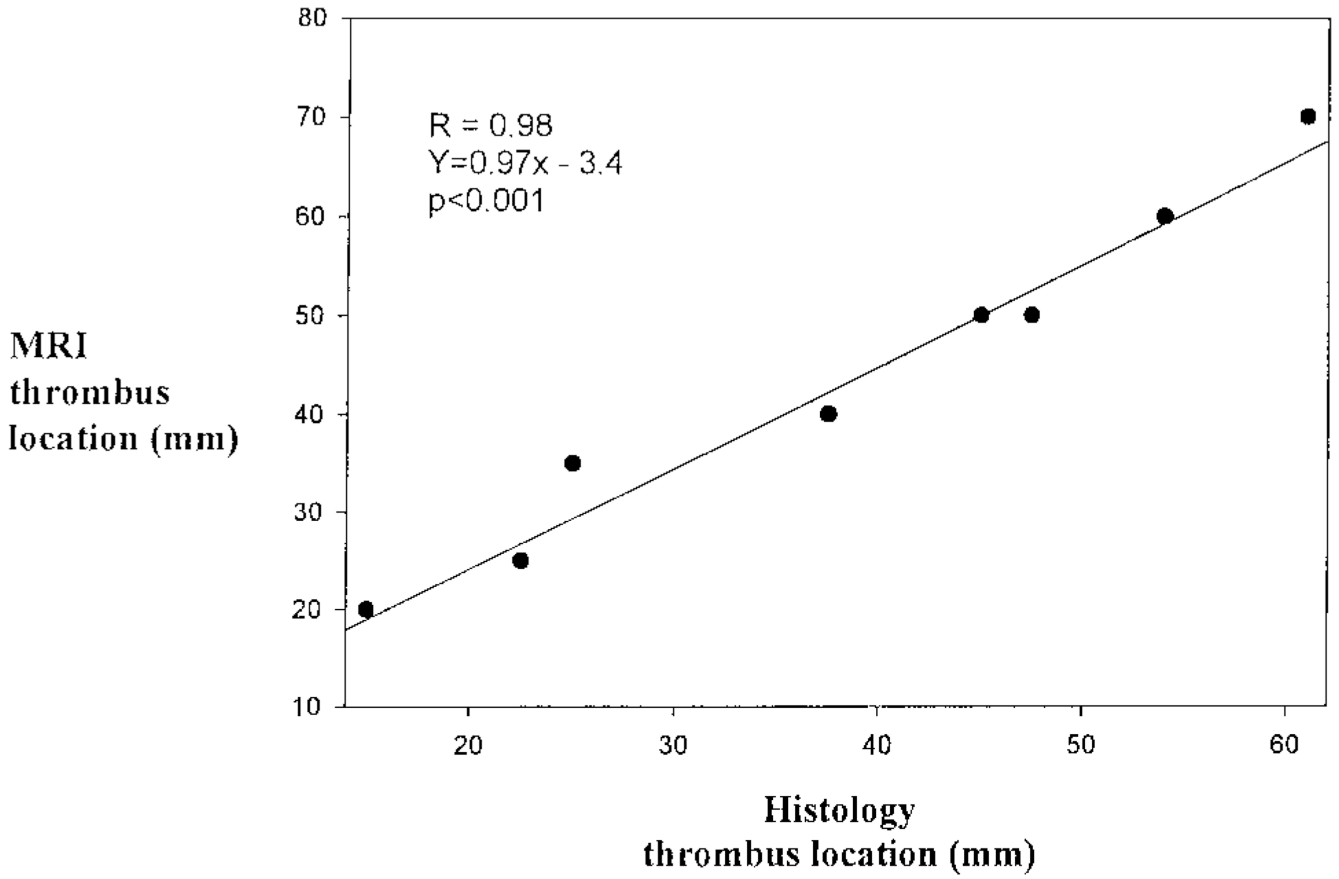

Figure 3.
Linear regression analysis comparing the location of the most distal portion of the thrombus from the right renal artery, as determined by MRI and histopathology.

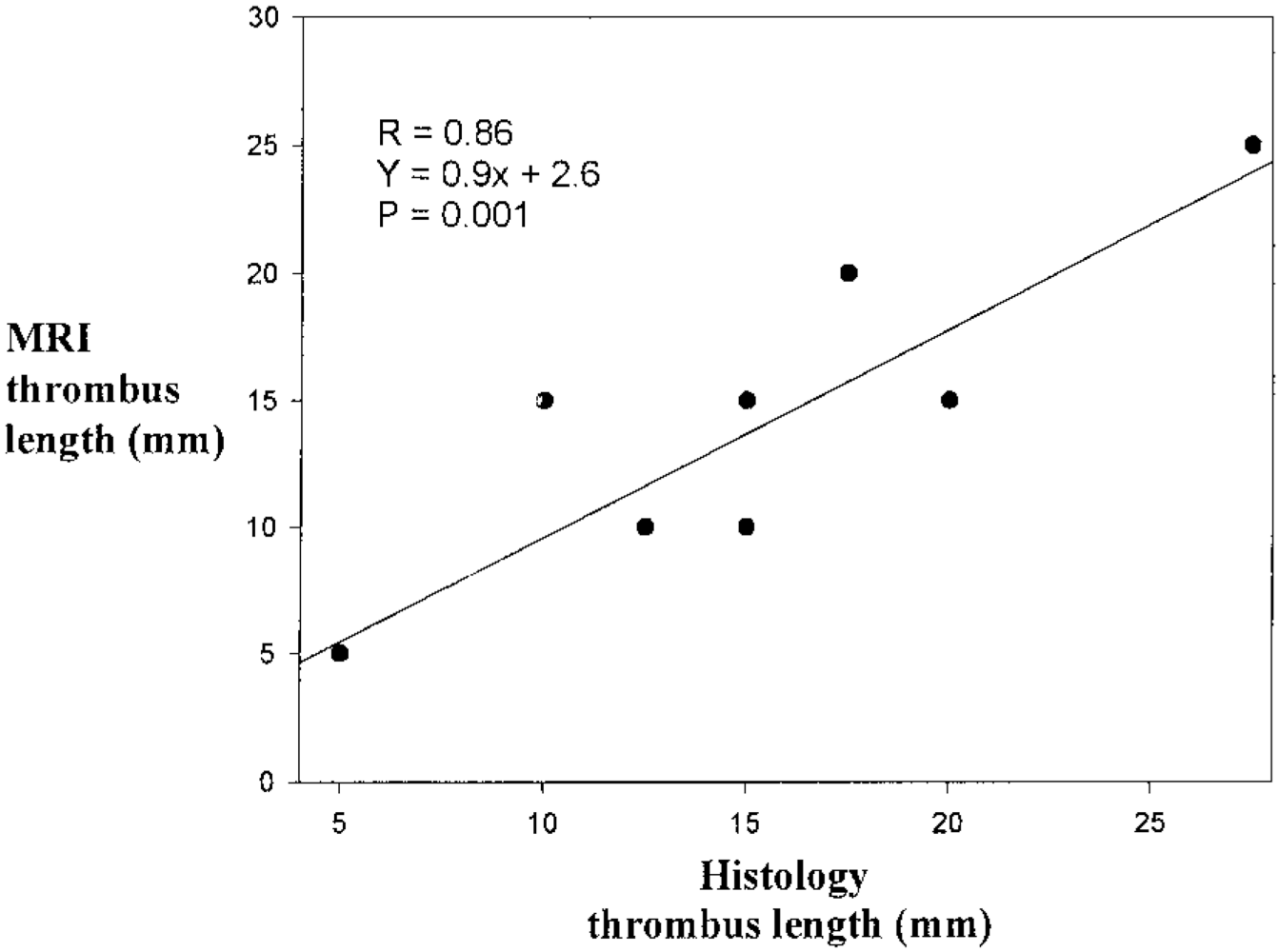

Figure 4.
Linear regression analysis comparing thrombus length, as determined by MRI and histopathology.